Hyperbolic relaxation models for thin films down an inclined plane

Firas Dhaouadi[a,1,*], Sergey Gavrilyuk[b], Jean-Paul Vila[c]

[a] *Institut de Mathématiques de Toulouse, UMR5219, Université de Toulouse, CNRS, Université Paul Sabatier, F-31062 Toulouse Cedex 9, France.*
[b] *Aix-Marseille University and CNRS UMR 7343 IUSTI, 5 rue Enrico Fermi, 13453 Marseille, France*
[c] *Institut de Mathématiques de Toulouse, UMR5219, Université de Toulouse, CNRS, INSA, F-31077 Toulouse, France*

Abstract

We present a family of relaxation models for thin films flows where both viscosity and surface tension effects are inherent. In a first step, a first-order hyperbolic approximation to the dissipationless part of the system is presented. The method is based on an augmented Lagrangian approach, where a classical penalty method is used and high-order derivatives in the Lagrangian are promoted to new independent variables, for which hyperbolic closure equations are sought. Then, we show that the viscous terms can be treated either by plugging them directly to the obtained system, making it of the hyperbolic-parabolic type or by casting them into an approximate algebraic source term that is asymptotically equivalent to the former formulation. Finally, the extension of the method to a classical nonlinear surface tension model is also presented. Numerical results, for all the proposed models are shown and compared with experimental results and reference solutions.

Keywords: Thin films, Fluid flows with Surface tension, First-order hyperbolic equations, Finite volumes.

1. Introduction

Thin films are ubiquitous in nature as well as in the modern life. Rain water flowing on windows or on car glass, develop patterns that are not only a sight to behold for the average observer, but also a topic of substantial interest for researchers in the last decades. In this context, the study of thin film flows aims mainly to provide equations which best describe the patterns and wavy motion that emerge in such fluids, which are too regular to be considered artifacts. However, as is generally the case in continuum mechanics, there is very often a compromise between the accuracy of a given model, its compatibility with the principles of physics and the ease of its resolution. For instance, a direct numerical simulation of the Navier-Stokes equations down to the smallest scales is extremely costly. This has motivated the development of a rich literature of approximate specific models, addressed to particular flow regimes with custom assumptions, cutting down computational costs and avoiding unnecessary complications when uncalled for.

For thin films flowing down an inclined plane, the first successful attempt to derive a consistent one-equation model was done by Benney [1]. The equation, obtained through an asymptotic expansion of the Navier-Stokes equations, is however known to have finite-time blow-ups. Since then, at least two-equations models have been sought. The earliest model can be traced back to Shkadov[2], motivated by the experimental results of Kapitza (Father & son) [3, 4]. Shkadov's model, compared to Benney's equation,

*Corresponding author
Email addresses: firas.dhaouadi@unitn.it (Firas Dhaouadi), sergey.gavrilyuk@univ-amu.fr (Sergey Gavrilyuk), vila@insa-toulouse.fr (Jean-Paul Vila)
[1] Present address: Department of Civil, Environmental and Mechanical Engineering, University of Trento, Via Mesiano 77, 38123 Trento, Italy.

does not have finite-time blow-ups and its validity extends to larger Reynolds numbers. Yet, it is not consistent with energy conservation. This inspired the development of several consistent two-equations models, many of which were analyzed and compared in [5], see also the references therein. It is worthy of note that recent advances are also considering consistent three-equations models, see for example [6] where an evolution equation for enstrophy (integral of the vorticity squared), was considered and shown to perform better than its two-equations counterpart.

In the current work, we do not propose a new model for thin films with surface tension, but we rather suggest an approach that approximates a certain class of existing models via a set of first-order hyperbolic equations, that are then easier to address from the numerical point of view. The idea of approximating PDEs by means of hyperbolic equations is becoming more of a trend in the recent years[7–12] . One of the main reasons is the rich literature of numerical methods that are being developed and optimized for first-order hyperbolic PDEs, allowing to solve the equations with high accuracy in reasonable amounts of time. The method we apply here, so-called augmented Lagrangian approach, was introduced in [13] for the Serre-Green-Naghdi equations, then successfully extended to the defocusing nonlinear Schrödinger equation [14]. The current paper, follows the same philosophy, as both thin films equations and the Schrödinger equation, written under Madelung variables[15], fall into the same broader category of Euler-Korteweg equations. Since the times of Van der Waals [16] and Lord Rayleigh [17], this system of equations has been the subject of several contributions, out of which a non-exhaustive selection is recalled here [18–27]. In the context of our approach, the equations are still derived from a variational principle and admit an additional scalar conservation equation for the corresponding total energy. The approach is shown to work even in the presence of inherent dissipative terms. We show in particular that one can make use of Rayleigh's dissipation functions to cast parabolic viscous terms into algebraic approximations, thus conserving a fully hyperbolic structure even in this case.

This paper is organized as follows. Section 1 recalls the general structure of the systems we are concerned about. Details on how the augmented Lagrangian method works are then given, supported by a general proof of hyperbolicity of the thus obtained equations. Section 2 lays out the setting and the specific details of the thin films model, which will serve as a basis for the numerical tests. Two methods on how to add the parabolic viscous term are given therein followed by a comparison of the stability properties of both the augmented model and the original one. Section 3 provides all the necessary details of the finite volume numerical method, followed by a set of test cases for the Liu & Gollub's experiment. Comparisons with the experimental results are provided and a comparison of the different approaches for viscosity are also shown. A test case for a nonlinear surface tension formulation is presented at the end. Additional theoretical developments are included in the appendixes A to C, at the end of this paper.

2. Augmented Lagrangian framework

2.1. Reference system

The approach we present here concerns any shallow water system in which surface tension effects are inherent. Generally, we are considering systems that can be derived from a Lagrangian of the form

$$\mathcal{L} = \int_{\Omega_t} \left(\frac{1}{2} h|\mathbf{u}|^2 - f(h) - \frac{\sigma}{2\rho}|\nabla h|^2 \right) d\Omega. \tag{1}$$

Here, $h = h(\mathbf{x}, t) > 0$ is the fluid depth and $\mathbf{u}(\mathbf{x}, t)$ is the velocity field. $f(h)$ is an arbitrary function of the fluid depth, assumed convex and positive, σ is the surface tension coefficient and ρ is the fluid density. The corresponding Euler-Lagrange equations under the mass conservation constraint

$$\partial_t h + \nabla \cdot (h\mathbf{u}) = 0 \tag{2}$$

yield the momentum balance equation

$$\partial_t (h\mathbf{u}) + \nabla \cdot (h\mathbf{u} \otimes \mathbf{u}) + \nabla P = \nabla \cdot (\mathbf{K}). \tag{3}$$

where P is the hydrostatic pressure and $\mathbf{K}$ is the Korteweg stress tensor, both given by

$$P = hf'(h) - f(h), \quad \mathbf{K} = \left(\frac{\sigma}{2\rho}|\nabla h|^2 + \frac{\sigma}{\rho}h\Delta h\right)\mathbf{I} - \frac{\sigma}{\rho}\nabla h \otimes \nabla h. \tag{4}$$

Trivial calculus shows that $\nabla \cdot (\mathbf{K})$ reduces in this particular case to $\frac{\sigma}{\rho}h\nabla(\Delta h)$, so that the Euler-Korteweg system of shallow water equations writes in its simplest form

$$\partial_t(h) \quad + \nabla \cdot (h\mathbf{u}) = 0 \tag{5a}$$

$$\partial_t(h\mathbf{u}) + \nabla \cdot (h\mathbf{u} \otimes \mathbf{u}) + \nabla P = \frac{\sigma}{\rho}h\nabla(\Delta h). \tag{5b}$$

2.2. Augmented Lagrangian approach

The approach that we recall here finds its foundation in [14], in which more thorough details on the calculus of variations are given. Consider a new variable, say $\eta(\mathbf{x}, t)$ that is independent from the continuum. The idea is to introduce a relaxation in such a way that η tends towards h in the stiff relaxation limit so that we can use $\nabla\eta$ instead of ∇h in the surface tension term. To that end, let us introduce a new Lagrangian

$$\mathcal{L} = \int_{\Omega_t} \left(\frac{1}{2}h|\mathbf{u}|^2 - f(h) - \frac{\sigma}{2\rho}|\nabla\eta|^2 - \frac{1}{2\alpha h}(h-\eta)^2\right) d\Omega \tag{6}$$

where $\alpha > 0$ is a vanishing parameter. This new Lagrangian is non-other that the one introduced in (1) where ∇h was substituted by $\nabla\eta$, and a classical penalty term was added to ensure that the difference $(h-\eta)$ vanishes in the limit $\alpha \to 0$. One can see that the penalty coefficient is chosen to depend on the fluid depth h. This particular choice follows the discussion in [13] for the augmented Serre-Green-Naghdi equations, where it is shown that more trivial choices might result later in the loss of hyperbolicity or the cancellation of dispersive effects. With the introduction of the new independent degree of freedom η, the principle of stationary action applied to the Lagrangian (6) yields an additional Euler-Lagrange equation accounting for its variations:

$$\partial_t(h) \quad + \nabla \cdot (h\mathbf{u}) = 0 \tag{7a}$$

$$\partial_t(h\mathbf{u}) \quad + \nabla \cdot \left(h\mathbf{u} \otimes \mathbf{u} + \left(hf('h) - f(h) - \frac{\sigma}{2\rho}|\nabla\eta|^2 + \frac{\eta}{\alpha}\left(1 - \frac{\eta}{h}\right)\right)\mathbf{Id} + \frac{\sigma}{\rho}\nabla\eta \otimes \nabla\eta\right) = 0 \tag{7b}$$

$$-\frac{\sigma}{\rho}\Delta\eta = \frac{1}{\alpha}\left(1 - \frac{\eta}{h}\right). \tag{7c}$$

Equation (7c) shows that for sufficiently smooth solutions, $\eta \to h$ in the stiff limit. Besides, we can show that this system of equations is consistent with the reference Euler-Korteweg equations (5b) in the limit $\alpha \to 0$. In fact, it suffices to replace the term $\frac{\eta}{\alpha}\left(1 - \frac{\eta}{h}\right)$ in the momentum equation flux accordingly to equation (7c) to recover a more insightful formulation that writes:

$$\partial_t(h) \quad + \nabla \cdot (h\mathbf{u}) = 0 \tag{8a}$$

$$\partial_t(h\mathbf{u}) + \nabla \cdot (h\mathbf{u} \otimes \mathbf{u}) + \nabla P = \nabla \cdot (\mathbf{K}_1). \tag{8b}$$

$$\eta = h \quad + \alpha\frac{\sigma}{\rho}h\Delta\eta \tag{8c}$$

where $\mathbf{K_1}$ is given by

$$\mathbf{K_1} = \left(\frac{\sigma}{2\rho}|\nabla\eta|^2 + \frac{\sigma}{\rho}\eta\Delta\eta\right)\mathbf{I} - \frac{\sigma}{\rho}\nabla\eta \otimes \nabla\eta. \tag{9}$$

Note that $\mathbf{K_1}$ has exactly the same expression as the Korteweg stress tensor $\mathbf{K}$, only with h substituted by η. Furthermore, cast into this form, α no longer appears in the momentum equation. It only controls how

close η is to ρ through equation (8c). The latter, however, includes η on both sides of the equality sign, but can still be rearranged into a formal asymptotic expansion of η in powers of α with coefficients only depending on h up to leading order. This can be achieved by applying the Laplace operator to equation (8c) and repeatedly replacing $\Delta\eta$ up to any given order to obtain

$$\eta = h + \alpha\frac{\sigma}{\rho}h\Delta h + \alpha^2\frac{\sigma^2}{\rho^2}h\Delta(h\Delta h) + O(\alpha^3). \tag{10}$$

In the limit $\alpha \to 0$ one obtains $\eta \to h$ by virtue of the latter expansion. Consequently $\mathbf{K}_1 \to \mathbf{K}$ and we recover the original Euler-Korteweg equations, thus proving consistency of our system. However, up to this point, system of equations (8) does not seem to provide any easier formulation compared to the reference equations. Indeed, it bears close resemblance to the latter with the addition of a supplementary steady-state constraint which reduces the PDE order but does not make it any simpler, if not more complex. In an attempt to remedy to this complication, the idea is then to apply a second relaxation to the obtained constraint in order to cast it into a time-evolution equation. This can be carried out by further altering the Lagrangian (6) in the following way

$$\mathcal{L} = \int_{\Omega_t}\left(\frac{1}{2}h|\mathbf{u}|^2 - f(h) - \frac{\sigma}{2\rho}|\nabla\eta|^2 - \frac{1}{2\alpha h}(h-\eta)^2 + \frac{1}{2}\beta h\dot{\eta}^2\right)d\Omega \tag{11}$$

where an additional inertial term is added and β is a vanishing parameter governing the new relaxation. Given the structure of the modification, changes will only affect the constraint (7c) which now writes as a conservation law with a stiff source term:

$$\partial_t(h\dot{\eta}) + \nabla\cdot\left(h\dot{\eta}\mathbf{u} - \frac{\sigma}{\beta\rho}\nabla\eta\right) = \frac{1}{\alpha\beta}\left(1 - \frac{\eta}{h}\right). \tag{12}$$

It only remains to perform an order reduction of the system, by appointing new independent variables $\mathbf{p} = \nabla\eta$ and $w = \dot{\eta}$ and seeking suitable closure equations for the remaining degrees of freedom. These are obtained simply by writing the definition of w, which yields an evolution equation for η

$$\partial_t(\eta) + \mathbf{u}\cdot\nabla\eta = w, \tag{13}$$

and then applying the gradient operator to both sides of the equality to obtain an evolution equation for $\mathbf{p}$

$$\partial_t(\mathbf{p}) + \nabla(\mathbf{p}\cdot\mathbf{u} - w) = 0. \tag{14}$$

Thus, putting the equations altogether permits to obtain a closed set of conservation laws constituting the so-called augmented system of equations

$$\partial_t(h) \quad + \nabla\cdot(h\mathbf{u}) = 0 \tag{15a}$$

$$\partial_t(h\mathbf{u}) + \nabla\cdot(h\mathbf{u}\otimes\mathbf{u}) + \nabla P = \nabla\cdot(\mathbf{K}_2). \tag{15b}$$

$$\partial_t(h\eta) + \nabla\cdot(h\eta\mathbf{u}) = hw \tag{15c}$$

$$\partial_t(hw) + \nabla\cdot\left(hw\mathbf{u} - \frac{\sigma}{\beta\rho}\mathbf{p}\right) = \frac{1}{\alpha\beta}\left(1 - \frac{\eta}{h}\right) \tag{15d}$$

$$\partial_t(\mathbf{p}) \quad + \nabla(\mathbf{p}\cdot\mathbf{u} - w) = 0, \tag{15e}$$

with

$$\mathbf{K}_2 = \left(\frac{\sigma}{2\rho}|\mathbf{p}|^2 - \frac{\eta}{\alpha}\left(1 - \frac{\eta}{h}\right)\right)\mathbf{Id} - \frac{\sigma}{\rho}\mathbf{p}\otimes\mathbf{p}. \tag{16}$$

One can derive an additional conservation law for the total energy

$$E = \frac{1}{2}h|\mathbf{u}|^2 + f(h) + \frac{\sigma}{2\rho}|\mathbf{p}|^2 + \frac{1}{2\alpha h}(h-\eta)^2 + \frac{1}{2}\beta h w^2, \tag{17}$$

by summing all the equations of system (15), each multiplied by the corresponding entropic variable to obtain

$$\partial_t(E) + \nabla \cdot \left(E\mathbf{u} + (P\mathbf{Id} - \mathbf{K}_2)\,\mathbf{u} - \frac{\sigma}{\rho} w\mathbf{p} \right) = 0. \tag{18}$$

2.3. Hyperbolicity of the augmented system

In one dimension of space, system of equations (15e) can be cast into the quasilinear form

$$\partial_t(\mathbf{Q}) + \mathbf{A}(\mathbf{Q})\partial_x\mathbf{Q} = \mathbf{S}(\mathbf{Q}) \tag{19}$$

where $\mathbf{Q}$ is the vector of primitive variables, $\mathbf{A} = \mathbf{A}(\mathbf{Q})$ is the jacobian matrix of the flux, and $\mathbf{S} = \mathbf{S}(\mathbf{Q})$ is the vector of source terms, all of which are given by

$$\mathbf{A} = \begin{pmatrix} u & h & 0 & 0 & 0 \\ f''(h) + \frac{\eta^2}{\alpha h^3} & u & 0 & \frac{\sigma p}{\rho h} & \frac{1}{\alpha}\left(1 - \frac{2\eta}{h}\right) \\ 0 & 0 & u & -\frac{\sigma}{\beta\rho h} & 0 \\ 0 & p & -1 & u & 0 \\ 0 & 0 & 0 & 0 & u \end{pmatrix}, \quad \mathbf{Q} = \begin{pmatrix} h \\ u \\ w \\ p \\ \eta \end{pmatrix}, \quad \mathbf{S} = \begin{pmatrix} 0 \\ 0 \\ \frac{1}{\alpha\beta h}\left(1 - \frac{\eta}{h}\right) \\ 0 \\ w \end{pmatrix}. \tag{20}$$

$\mathbf{A}$ admits 5 eigenvalues that can be expressed as follows :

$$\xi = \begin{pmatrix} u \\ u + \sqrt{\psi_1 + \psi_2} \\ u + \sqrt{\psi_1 - \psi_2} \\ u - \sqrt{\psi_1 + \psi_2} \\ u - \sqrt{\psi_1 - \psi_2} \end{pmatrix} \text{ with } \begin{cases} \psi_1 = \frac{1}{2}(a^2 + a_\sigma^2 + a_\alpha^2 + a_\beta^2) \\ \psi_2 = \frac{1}{2}\sqrt{(a^2 + a_\sigma^2 + a_\alpha^2 - a_\beta^2)^2 + 4a_\beta^2 a_\sigma^2} \\ a = \sqrt{hf''(h)}, \quad a_\sigma = \sqrt{\dfrac{\sigma}{\rho h}p^2} \\ a_\alpha = \dfrac{\eta}{h\sqrt{\alpha}}, \quad a_\beta = \sqrt{\dfrac{\sigma}{\beta\rho h}} \end{cases} \tag{21}$$

Here a is the adiabatic sound speed of the hyperbolic part of the Euler-Korteweg system (5b), a_σ is the speed of propagation of waves of capillary nature, a_α and a_β are the fast wave speeds induced by the relaxation procedure. We will refer to them as the speed of first and second relaxation, respectively. The difference $\psi_1 - \psi_2$ can be shown positive since

$$\psi_2 = \sqrt{\psi_1^2 - a_\beta^2(a^2 + a_\alpha^2)} < \psi_1, \tag{22}$$

implying that the 5 eigenvalues are real. If $\psi_2 \neq 0$, then the system is strictly hyperbolic. Nevertheless, a full basis of 5 linearly independent right eigenvectors of the matrix $\mathbf{A}$ can still be computed. They are written as the columns of the following matrix, given from left to right in the same order as their corresponding eigenvalues:

$$\Lambda = \begin{pmatrix} -\frac{h-2\eta}{\alpha(\psi_1-\psi_3)} & -\frac{h(\psi_3+\psi_2)}{\psi_1-\psi_3} & -\frac{h(\psi_3+\psi_2)}{\psi_1-\psi_3} & \frac{h(\psi_2-\psi_3)}{p(\psi_1-\psi_3)} & \frac{h(\psi_2-\psi_3)}{p(\psi_1-\psi_3)} \\ 0 & \frac{\psi_4+\psi_2}{\sqrt{\psi_1-\psi_2}} & -\frac{\psi_4+\psi_2}{\sqrt{\psi_1-\psi_2}} & -\frac{\psi_2-\psi_4}{p\sqrt{\psi_1+\psi_2}} & \frac{\psi_2-\psi_4}{p\sqrt{\psi_1+\psi_2}} \\ 0 & \frac{(\psi_1+\psi_4)p}{\sqrt{\psi_1-\psi_2}} & -\frac{(\psi_1+\psi_4)p}{\sqrt{\psi_1-\psi_2}} & \frac{\psi_1+\psi_4}{\sqrt{\psi_1+\psi_2}} & -\frac{\psi_1+\psi_4}{\sqrt{\psi_1+\psi_2}} \\ 0 & p & p & 1 & 1 \\ 1 & 0 & 0 & 0 & 0 \end{pmatrix}, \quad \det(\Lambda) = \frac{16ha_\beta\psi_2^2}{(a^2 + a_\alpha^2)^{\frac{3}{2}}} > 0 \tag{23}$$

where ψ_3 and ψ_4 are functions of the wave speeds given by

$$\psi_3 = \frac{1}{2}(a_\beta^2 + a_\sigma^2 - a^2 - a_\alpha^2), \quad \psi_4 = \frac{1}{2}(a_\beta^2 - a_\sigma^2 - a^2 - a_\alpha^2). \tag{24}$$

Now, in the case where $\psi_2 = 0$, the system loses strict hyperbolicity as some eigenvalues coincide with one another. This occurs when both of the following conditions are met simultaneously:

$$p = 0, \tag{25a}$$

$$hf''(h) + \frac{\eta^2}{\alpha h^2} = \frac{\sigma}{\beta\rho h} \tag{25b}$$

Even in this case, we still obtain a full set of linearly independent right eigenvectors and the eigensystem of A writes

$$\xi = \begin{pmatrix} u \\ u + \sqrt{\psi_1} \\ u + \sqrt{\psi_1} \\ u - \sqrt{\psi_1} \\ u - \sqrt{\psi_1} \end{pmatrix}, \quad \Lambda = \begin{pmatrix} -\frac{h-2\eta}{\alpha a_\beta^2} & 0 & \frac{h}{a_\beta} & 0 & -\frac{h}{a_\beta} \\ 0 & 0 & 1 & 0 & 1 \\ 0 & -a_\beta & 0 & a_\beta & 0 \\ 0 & 1 & 0 & 1 & 0 \\ 1 & 0 & 0 & 0 & 0 \end{pmatrix}. \tag{26}$$

Thus, system of equations (19) is unconditionally hyperbolic. The analysis in many dimensions of space is out of the scope of this work. Nevertheless, it is important to point out that system of equations (15), written as is, is not strongly hyperbolic in the multi-dimensional case. It needs to be cast into a Galilean invariant form and supplemented by an additional evolution equation that enforces the curl-free constraint at the discrete level, imposed by definition on the vector $\mathbf{p} = \nabla\eta$. The procedure, called Generalized Lagrange multiplier curl-cleaning, turns out to also restore the strong hyperbolicity of the augmented system [28].

2.4. Case of nonlinear surface tension terms

In most of the models considering thin film flows with surface tension, capillary energy is taken quadratic in $|\nabla h|$. More rigorous formulations consider a nonlinear term accounting for capillary energy that reads

$$e_{cap} = \frac{\sigma}{\rho}\left(\sqrt{1 + |\nabla h|^2} - 1\right), \tag{27}$$

from which, the classical quadratic formulation can be obtained by expanding in series of $|\nabla h|$ and keeping the leading order terms. While this approximation is generally satisfactory, it becomes less reliable in the case where large gradients of fluid height are involved. Thus, it seems important to address such a case, especially that in the framework of the augmented Lagrangian approach, no additional efforts are to be invested. Indeed, the augmented system energy writes in this case:

$$E = h\frac{|\mathbf{u}|^2}{2} + f(h) + \frac{\sigma}{\rho}\left(\sqrt{1 + |\mathbf{p}|^2} - 1\right) + \frac{1}{\alpha h}(h - \eta)^2 + \frac{1}{2}\beta h w^2 \tag{28}$$

Being in the same setting as before, the modification of capillary energy only affects equations (15b) and (15d) which now read:

$$\partial_t(h\mathbf{u}) + \nabla \cdot (h\mathbf{u} \otimes \mathbf{u}) + \nabla P = \nabla \cdot (\mathbf{K}_2') \tag{29a}$$

$$\partial_t(hw) + \nabla \cdot \left(hw\mathbf{u} - \frac{\sigma}{\beta\rho}\frac{\mathbf{p}}{\sqrt{1 + |\mathbf{p}|^2}}\right) = \frac{1}{\alpha\beta}\left(1 - \frac{\eta}{h}\right) \tag{29b}$$

where $\mathbf{K}_2'$ is given by

$$\mathbf{K}_2' = \left(\frac{\sigma}{\rho}\sqrt{1 + |\mathbf{p}|^2} - \frac{\eta}{\alpha}\left(1 - \frac{\eta}{h}\right)\right)\mathbf{Id} - \frac{\sigma}{\rho}\frac{\mathbf{p} \otimes \mathbf{p}}{\sqrt{1 + |\mathbf{p}|^2}}. \tag{30}$$

In one dimension of space, the eigenstructure of the system of equations is identical to (21), with minor changes in a_σ and a_β which in this case write

$$a_\sigma = \sqrt{\frac{\sigma p^2}{\rho h(1 + p^2)^{3/4}}}, \quad a_\beta = \sqrt{\frac{\sigma}{\beta\rho h(1 + p^2)^{3/4}}}. \tag{31}$$

The system is thus hyperbolic by virtue of the same analysis provided in the previous section.

3. Application to thin film flows with capillarity

3.1. Reference model, setting and notations

We consider a thin film that flows over an inclined horizontal plate under the effects of gravity:

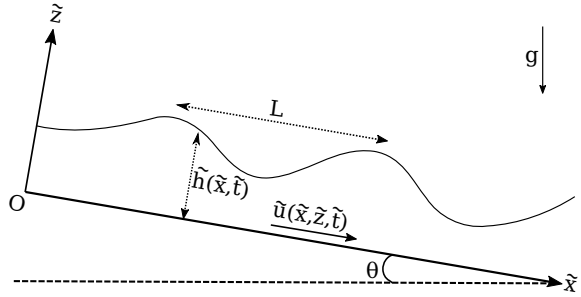

Figure 1: Schematic of a flowing thin film over an inclined horizontal plate with the notations used in this section.

Here, the 'tilde' infers that the associated quantity is dimensioned. $\tilde{h}(\tilde{x},\tilde{t})$ refers to the fluid height and $\tilde{u}(\tilde{x},\tilde{z},\tilde{t})$ is the local velocity. The $\tilde{x}$ and $\tilde{z}$ respectively denote the directions parallel and normal to the plane. The transverse direction $\tilde{y}$ is neglected, as the applications considered here exhibit mainly two-dimensional dynamics. The angle θ is the constant inclination of the plate and g is the acceleration of gravity. The typical distance in the $\tilde{x}$ direction will be denoted by L. For periodic waves, this refers to the wavelength. In the long wave approximation, the ratio ε between the typical depth and wavelength is assumed to be small.

In order to obtain a non-dimensional form of the equations, one needs to consider some scaling of reference. For that, let us consider the *Nusselt flow* solution. It corresponds to the equilibrium solution, balancing the viscous forces and the gravity forces, resulting in a semi-parabolic velocity profile

$$\begin{cases} \tilde{h}(\tilde{x},\tilde{t}) = \tilde{h}_N \\ \tilde{u}(\tilde{x},\tilde{z},\tilde{t}) = \tilde{u}_N(z) = \dfrac{g}{\nu}\sin\theta\tilde{z}\left(\tilde{h}_N - \dfrac{\tilde{z}}{2}\right). \end{cases} \tag{32}$$

The velocity is dependent on the fluid height and thus, in order to obtain a relevant characteristic velocity, we can average it over the depth. For the sake of lightness, the averaged velocity will be denoted by its uppercase equivalent:

$$\tilde{U}_N = \frac{1}{\tilde{h}_N}\int_0^{\tilde{h}_N} \tilde{u}_N(\tilde{z})d\tilde{z} = \frac{g\tilde{h}_N^2}{3\nu}\sin\theta \tag{33}$$

Using this reference solution, we can define the Reynolds number Re, the Froude number F and the Weber number We by

$$Re = \frac{\tilde{h}_N\tilde{U}_N}{\nu}, \quad F = \frac{\tilde{U}_N}{\sqrt{g\tilde{h}_N}}, \quad We = \frac{\rho}{\sigma}\tilde{h}_N\tilde{U}_N^2, \tag{34}$$

and the long wave parameter by

$$\varepsilon = \frac{\tilde{h}_N}{L}. \tag{35}$$

Thus, this permits to obtain the dimensionless quantities

$$u = \frac{\tilde{u}}{\tilde{U}_N}, \quad U = \frac{\tilde{U}}{\tilde{U}_N}, \quad h = \frac{\tilde{h}}{\tilde{h}_N}, \quad x = \frac{\tilde{x}}{L}, \quad z = \frac{\tilde{z}}{\tilde{h}_N}, \quad t = \frac{\tilde{t}}{L}\tilde{U}_N. \tag{36}$$

Under these notations, we will consider a particular two-equation model for thin film flows [29, 5, 6] and which writes

$$\partial_t h + \partial_x(hU) = 0 \tag{37a}$$

$$\partial_t(hU) + \partial_x\left(hU^2 + \frac{2\lambda^2}{225}h^5 + \frac{\cos\theta}{2F^2}h^2\right) - \frac{\varepsilon^2\kappa}{F^2}hh_{xxx} = \frac{1}{\varepsilon Re}\left(\lambda h - \frac{3U}{h}\right) + \frac{9\varepsilon}{2Re}\partial_x(hU_x), \tag{37b}$$

where the dimensionless parameters λ, and κ are introduced for convenience, as in [6] and are defined by:

$$\lambda = \frac{Re\sin\theta}{F^2}, \quad \kappa = \frac{F^2}{We} \tag{38}$$

Equations (37) admit dissipative algebraic source terms at leading order in ε, as well as a viscous parabolic term. The left-hand side however is conservative and can be regarded as the Euler-Lagrange equations to the Lagrangian

$$\mathcal{L} = \int_{\Omega_t}\left(\frac{1}{2}hU^2 - f(h) - \frac{\varepsilon^2\kappa}{2F^2}h_x^2\right)d\Omega, \quad \text{with} \quad f(h) = \frac{h^2\cos\theta}{2F^2} + \frac{\lambda^2h^5}{450}. \tag{39}$$

This Lagrangian will serve as the basis for the hyperbolic relaxation method. Thus, the right-hand side in the system of equations (37) will be omitted in the process and then added back only after the augmented system of equations has been established.

3.2. Augmented model

The augmented Lagrangian in this case writes

$$\mathcal{L} = \int_{\Omega_t}\left(\frac{1}{2}hU^2 - f(h) - \frac{\varepsilon^2\kappa}{2F^2}\eta_x^2 - \frac{1}{\alpha h}(h-\eta)^2 + \frac{1}{2}\beta h\dot{\eta}^2\right)d\Omega. \tag{40}$$

The corresponding Euler-Lagrange equations, taking into account the acceleration of gravity, are given by

$$\partial_t(h) \quad + \partial_x(hU) = 0 \tag{41a}$$

$$\partial_t(hU) + \partial_x\left(hU^2 + \frac{2\lambda^2}{225}h^5 + \frac{\cos\theta}{2F^2}h^2 + \frac{\eta}{\alpha}\left(1-\frac{\eta}{h}\right) + \frac{\varepsilon^2\kappa}{2F^2}p^2\right) = \frac{\lambda h}{\varepsilon Re} \tag{41b}$$

$$\partial_t(h\eta) \quad + \partial_x(h\eta U) = hw \tag{41c}$$

$$\partial_t(hw) + \partial_x\left(hwU - \frac{\varepsilon^2\kappa}{\beta F^2}p\right) = \frac{1}{\alpha\beta}\left(1-\frac{\eta}{h}\right) \tag{41d}$$

$$\partial_t(p) \quad + \partial_x(pU - w) = 0 \tag{41e}$$

These equations are hyperbolic and the corresponding wave speeds write

$$\xi = \begin{pmatrix} U \\ U + \sqrt{\psi_1 + \psi_2} \\ U + \sqrt{\psi_1 - \psi_2} \\ U - \sqrt{\psi_1 + \psi_2} \\ U - \sqrt{\psi_1 - \psi_2} \end{pmatrix} \text{ with } \begin{cases} \psi_1 = \frac{1}{2}(a^2 + a_\sigma^2 + a_\alpha^2 + a_\beta^2) \\ \psi_2 = \frac{1}{2}\sqrt{(a^2 + a_\sigma^2 + a_\alpha^2 - a_\beta^2)^2 + 4a_\beta^2 a_\sigma^2} \\ a = \sqrt{\frac{h\cos\theta}{F^2} + \frac{2\lambda^2h^4}{45}}, \quad a_\sigma = \sqrt{\frac{\kappa\varepsilon^2}{hF^2}p^2} \\ a_\alpha = \frac{\eta}{h\sqrt{\alpha}}, \quad a_\beta = \sqrt{\frac{\kappa\varepsilon^2}{\beta hF^2}}. \end{cases} \tag{42}$$

3.3. Appending dissipative terms

The last step is to account for the dissipative terms which were up to now disregarded. One way would be to insert the omitted right-hand side term of the momentum equation of system (37), back into the augmented system (41) which results in a mixed hyperbolic-parabolic PDE given by

$$\partial_t(h) \quad + \partial_x(hU) = 0 \tag{43a}$$

$$\partial_t(hU) + \partial_x\left(hU^2 + \frac{2\lambda^2 h^5}{225} + \frac{h^2\cos\theta}{2F^2} + \frac{\eta}{\alpha}\left(1-\frac{\eta}{h}\right) + \frac{\varepsilon^2\kappa}{2F^2}p^2\right) = \frac{1}{\varepsilon Re}\left(\lambda h - \frac{3U}{h}\right) + \frac{9\varepsilon}{2Re}\partial_x(h\partial_x U) \tag{43b}$$

$$\partial_t(h\eta) \; + \partial_x(h\eta U) = hw \tag{43c}$$

$$\partial_t(hw) + \partial_x\left(hwU - \frac{\varepsilon^2\kappa}{\beta F^2}p\right) = \frac{1}{\alpha\beta}\left(1-\frac{\eta}{h}\right) \tag{43d}$$

$$\partial_t(p) \quad + \partial_x(pU - w) = 0 \tag{43e}$$

An alternative approach that maintains the hyperbolic structure of the whole system would be to include the non-conservative forces into the Euler-Lagrange equations, in a way that is asymptotically compatible with the parabolic vicous term $\frac{9\varepsilon}{2Re}\partial_x(h\partial_x U)$, introduced in equation (43). This can be done by using the Rayleigh dissipation function [30], allowing us to cast friction forces into algebraic sources. In our case, an appropriate choice of the Rayleigh function would be

$$\mathcal{R} = \frac{3u^2}{2h\varepsilon Re} + \frac{9\varepsilon w^2}{4\eta Re}. \tag{44}$$

Deriving the Euler-Lagrange equations and including the function $\mathcal{R}$ permits to obtain the equations (see Appendix B)

$$\partial_t(h) \quad + \partial_x(hU) = 0 \tag{45a}$$

$$\partial_t(hU) + \partial_x\left(hU^2 + \frac{2\lambda^2}{225}h^5 + \frac{\cos\theta}{2F^2}h^2 + \frac{\eta}{\alpha}\left(1-\frac{\eta}{h}\right) + \frac{\varepsilon^2\kappa}{2F^2}p^2\right) = \frac{\lambda h}{\varepsilon Re} - \frac{3U}{h\varepsilon Re} \tag{45b}$$

$$\partial_t(h\eta) \; + \partial_x(h\eta U) = hw \tag{45c}$$

$$\partial_t(hw) + \partial_x\left(hwU - \frac{\varepsilon^2\kappa}{\beta F^2}p\right) = \frac{1}{\alpha\beta}\left(1-\frac{\eta}{h}\right) - \frac{9\varepsilon w}{2\beta\eta Re} \tag{45d}$$

$$\partial_t(p) \quad + \partial_x(pU - w) = 0 \tag{45e}$$

At this point, independently on the chosen formulation, we end up with a system of equations in which the two relaxation parameters α and β appear along ε, which governs the asymptotic derivation of the original equations (37). Thus, a possible preliminary scaling of the relaxation parameters should be such as not to disrupt the asymptotic expansion down to the lowest order present in the equations. It can be shown (see Appendix A), that this requirement can be met if we take

$$\beta = O(\varepsilon^3). \tag{46}$$

The fact that no restrictions appear on the parameter α, is because the momentum equation only involves the latter when it comes to surface tension terms whose coefficient is quadratic in ε, thus shifting the corresponding error to a higher order in ε. Nevertheless, the choice of α will be considered in the next part when calibrating neutral stability curves.

3.4. Linearized stability analysis

Another important property of the model to be checked is its stability curve. If the neutral stability curves of both systems are significantly different, then discrepancies in their respective behaviors may be

observed for the same frequencies. Unstable waves in the original system could become stable for the augmented model or vice-verse. Thus, in order to avoid such an inconsistency, it is necessary to compute the dispersion relation. This will be done for one example in order to show that stability properties are well-approximated by the augmented Lagrangian procedure. In this example, the parabolic diffusion terms are omitted, as they unnecessarily encumber the expressions without adding any substantial information to the analysis. We proceed by casting the system into quasi-linear form

$$\partial_t(\mathbf{Q}) + \mathbf{A}(\mathbf{Q})\partial_x(\mathbf{Q}) = \mathbf{S}(\mathbf{Q}) \tag{47}$$

where :

$$\mathbf{Q} = \begin{pmatrix} h \\ U \\ \eta \\ w \\ p \end{pmatrix}, \ \mathbf{A}(\mathbf{Q}) = \begin{pmatrix} U & h & 0 & 0 & 0 \\ \frac{\cos\theta}{F^2} + \frac{2\lambda^2 h^3}{45} + \frac{\eta^2}{\alpha h^3} & U & \frac{1}{\alpha}\left(1 - \frac{2\eta}{h}\right) & 0 & \frac{\varepsilon^2\kappa p}{F^2 h} \\ 0 & 0 & U & 0 & 0 \\ 0 & 0 & 0 & U & -\frac{\varepsilon^2\kappa}{\beta F^2 h} \\ 0 & p & 0 & -1 & U \end{pmatrix}, \mathbf{S}(\mathbf{Q}) = \begin{pmatrix} 0 \\ \frac{\lambda h}{\varepsilon Re} - \frac{3U}{\varepsilon h Re} \\ w \\ \frac{1}{\alpha\beta h}\left(1 - \frac{\eta}{h}\right) \\ 0 \end{pmatrix} \tag{48}$$

We consider an equilibrium state $\mathbf{Q}_0 = (h_0, u_0, h_0, 0, 0)^T$, and look for solutions which are proportional to $e^{i(kx-wt)}$. As a reference solution, we can choose the Nusselt flow solution ($h_0 = 1, u_0 = 1$). The phase velocity $c_p = \omega/k$ is then an eigenvalue of the matrix

$$\mathbf{M} = \mathbf{A}(\mathbf{Q_0}) + \frac{i}{k}\nabla_{\mathbf{Q}}(\mathbf{S}(\mathbf{Q}_0)). \tag{49}$$

In the context of our analysis, since we would like to compare neutral stability curves, we only need to look for the critical stability line defined by $\mathrm{Im}(c_p) = 0$. Solving this equation yields the expression for the latter (See Appendix C) and which writes

$$\frac{\kappa k^2}{\sin\theta} + \mathrm{cotg}\theta - \frac{6}{5}Re + \left(\alpha\left(4\beta - \frac{\kappa}{F^2}\right)\left(\frac{6}{5}Re - \mathrm{cotg}\theta\right) - 4\beta\frac{F^2}{\sin\theta}\right)k^2 = 0 \tag{50}$$

This equation is consistent, in the limits $\alpha \to 0$ and $\beta \to 0$, with the well-known stability condition of the original equations (37)

$$\frac{\kappa k^2}{\sin\theta} + \mathrm{cotg}\theta - \frac{6}{5}Re = 0. \tag{51}$$

The error terms in equation (50) are quadratic in k, implying that convergence is not uniform with respect to the latter. This is confirmed in figure 2 where neutral stability curves for the original system and the augmented one are compared for several values of α and β. The values which were obtained through the asymptotic analysis show a very good agreement in terms of stability regions. Less restrictive values of either α or β are shown to exhibit a different behavior in the sense that the instability region in these cases is significantly wider. In terms of convergence, it is clear that for low frequencies the curves match very well up to a certain cut-off frequency, starting from which there is a notable increase in the error of approximation. For the range of Reynolds numbers of interest for us, we will continue with the values $\alpha = \varepsilon$ and ε^3 as they provide a very close approximation to the stability properties as shown in figure 2.

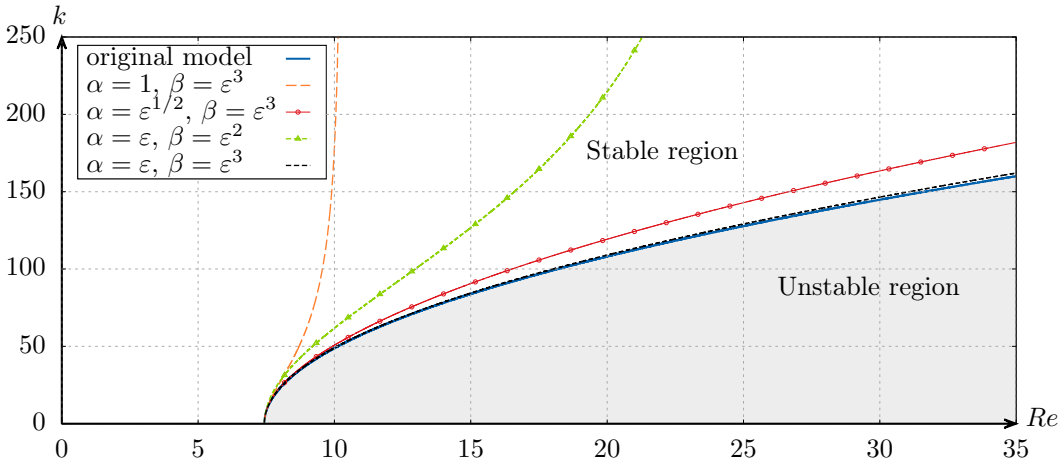

Figure 2: Neutral stability curves in the (k, Re) plane for the original model (continuous blue line) and the augmented model for various scalings of α and β with respect to ε. The parameters used here correspond to the Liu & Gollub's experiments [31] with $\theta = 6.4°, We = 0.184, F = 0.847$ and $\varepsilon = 0.006$.

4. Numerical simulations

4.1. Numerical method

In this part we lay out all the necessary details related to the numerical resolution of both systems (45) and (43). While the former is of purely hyperbolic nature, the latter admits an additional parabolic term. The idea is then to use a common finite volume method for both systems, and simply apply explicit centered finite differences to discretize the diffusion operator that appears in the hyperbolic-parabolic formulation. In the finite volume framework, we consider the system to solve in its conservative form

$$\partial_t \mathbf{U} + \partial_x \left(\mathbf{F}(\mathbf{U})\right) = \mathbf{S}(\mathbf{U}). \tag{52}$$

The PDE is solved on a discretization of a given domain $[x_L, x_R] \times [0, T]$, denoted by

$$x_i = x_L + \left(i - \frac{1}{2}\right)\Delta x, \quad t^n = n\Delta t, \quad i \in [1, N],\ n \in [0, n_{max}],\ \Delta x = \frac{x_R - x_L}{N} \tag{53}$$

where x_i represents the center of the *ith* cell. In these notations, a local space-time control volume is delimited by $[x_i - \frac{\Delta x}{2},\ x_i + \frac{\Delta x}{2}] \times [t^n,\ t^{n+1}]$. We will consider in our case a second-order accurate ARS(2,2,2)[32] discretization of (52). The scheme is based on an Implicit-Explicit (IMEX) decomposition of the system, that is well-adapted for stiff source terms. We recall below the corresponding Butcher tableaux [32]

$$\begin{array}{c|ccc} 0 & 0 & 0 & 0 \\ \gamma & \gamma & 0 & 0 \\ 1 & \delta & 1-\delta & 0 \\ \hline & \delta & 1-\delta & 0 \end{array}, \quad \begin{array}{c|ccc} 0 & 0 & 0 & 0 \\ \gamma & 0 & \gamma & 0 \\ 1 & 0 & 1-\gamma & \gamma \\ \hline & 0 & 1-\gamma & \gamma \end{array}, \quad \begin{cases} \gamma = 1 - \dfrac{1}{\sqrt{2}} \\ \delta = 1 - \dfrac{1}{2\gamma} \end{cases} \tag{54}$$

where the left table corresponds to the explicit part and the right one to the implicit part. When applied to the conservative equation (52), with initial condition $\mathbf{U}_i^n$ this yields the two-stage scheme

$$\mathbf{U}_i^\star = \mathbf{U}_i^n + \gamma\Delta t\left(-\frac{\mathbf{F}^n_{i+\frac{1}{2}} - \mathbf{F}^n_{i-\frac{1}{2}}}{\Delta x} + \mathbf{S}(\mathbf{U}_i^\star)\right) \tag{55a}$$

$$\mathbf{U}_i^{n+1} = \mathbf{U}_i^n - \Delta t\left(\delta\frac{\mathbf{F}^n_{i+\frac{1}{2}} - \mathbf{F}^n_{i-\frac{1}{2}}}{\Delta x} + (1-\delta)\frac{\mathbf{F}^\star_{i+\frac{1}{2}} - \mathbf{F}^\star_{i-\frac{1}{2}}}{\Delta x}\right) + \Delta t\left((1-\gamma)S(\mathbf{U}_i^\star) + \gamma S(\mathbf{U}_i^{n+1})\right), \tag{55b}$$

where $\mathbf{F}^n_{i+\frac{1}{2}}$ is an intercell flux, computed by using a classical Riemann solver. In our case we use the Rusanov flux [33]

$$\mathbf{F}^n_{i+\frac{1}{2}} = \frac{1}{2}\left(\mathbf{F}(\mathbf{w}^L_{i+1}) + \mathbf{F}(\mathbf{w}^R_i)\right) - \frac{1}{2}s^{max}_{i+\frac{1}{2}}\left(\mathbf{w}^L_{i+1} - \mathbf{w}^R_i\right) \tag{56}$$

where $\mathbf{w}^L_i$ (resp. $\mathbf{w}^R_i$) is the boundary extrapolated value to the left (resp. to the right) of a piece-wise linear reconstruction $\mathbf{w}^n_i(x)$, obtained from $\mathbf{U}^n_i$ through the MUSCL approach [33, 34]. For every cell, $s^{max}_{i+\frac{1}{2}}$ is evaluated by using

$$s^{max}_{i+\frac{1}{2}} = \max\left(\max_{1\le j\le 5}\left(\left|\xi_j(\mathbf{U}^L_{i+1})\right|\right), \max_{1\le j\le 5}\left(\left|\xi_j(\mathbf{U}^R_i)\right|\right)\right) \tag{57}$$

where ξ_j are the eigenvalues of the flux Jacobian. In the scheme (55), the source terms are to be resolved implicitly. This suggests the use of either root-finding algorithms (e.g. Newton-Raphson or fixed-point iterations), or solving the algebraic equation by hand, which in this case is a feasible task. In the case where we are numerically solving equations (43), we only need to add the discretized parabolic viscous term $\mathbf{D}^n_i$ to the scheme (55) as follows

$$\mathbf{U}^\star_i = \mathbf{U}^n_i + \gamma\Delta t\left(-\frac{\mathbf{F}^n_{i+\frac{1}{2}} - \mathbf{F}^n_{i-\frac{1}{2}}}{\Delta x} + \mathbf{D}^n_i + \mathbf{S}(\mathbf{U}^\star_i)\right)$$

$$\mathbf{U}^{n+1}_i = \mathbf{U}^n_i - \Delta t\left(\delta\frac{\mathbf{F}^n_{i+\frac{1}{2}} - \mathbf{F}^n_{i-\frac{1}{2}}}{\Delta x} - \delta\mathbf{D}^n_i + (1-\delta)\frac{\mathbf{F}^\star_{i+\frac{1}{2}} - \mathbf{F}^\star_{i-\frac{1}{2}}}{\Delta x} - (1-\delta)\mathbf{D}^\star_i\right) + \Delta t\left((1-\gamma)S(\mathbf{U}^\star_i) + \gamma S(\mathbf{U}^{n+1}_i)\right),$$

where $\mathbf{D}^n_i = (0, d^n_i, 0, 0, 0)^T$, and d^n_i is given by

$$d^n_i = \frac{9\varepsilon}{4Re\Delta x^2}((h^n_i + h^n_{i+1})(U^n_{i+1} - U^n_i) - (h^n_i + h^n_{i-1})(U^n_i - U^n_{i-1})). \tag{59}$$

In this case, the scheme is stable with a CFL condition of the form

$$\max\left(\xi_{max}\frac{\Delta t}{\Delta x}, \frac{9\varepsilon}{Re}\frac{\Delta t}{\Delta x^2}\right) \le 1 \tag{60}$$

4.2. Liu & Gollub's experiment

We study here the experiments done by Liu and Gollub [31]. It consists in a two-meter long canal, inclined with a constant angle θ, containing a thin film of an aqueous solution of glycerin (around one millimeter). The fluid is initially at rest. At $t = 0$, a periodic perturbation, with an arbitrary amplitude, is imposed at one of its boundaries. Depending on the frequency of the perturbation, the thus generated waves have amplitudes that may decay or grow in time. The frequencies of interest in this experiment are the unstable frequencies, for which it was observed that the wave amplitude grows until it reaches a stationary state whose behavior is strongly dependent on the imposed frequency. An example is given in figure 3 for a frequency of $1.5Hz$. The perturbation is imposed on the left boundary. One can see that the initial oscillations grow as they propagate until a wave-train of small capillary oscillations appears in the vicinity of the leading front which stabilizes the time evolution.

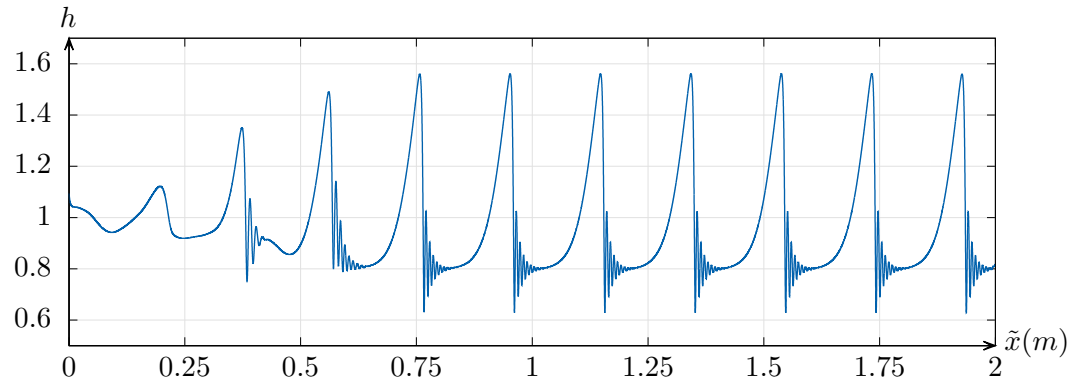

Figure 3: Dimensionless water height as a function of space (dimensioned), in the setting of the Liu & Gollub experiment, for an imposed frequency of $1.5Hz$. (Obtained through numerical simulation). Parameters used here are : $Re = 19.33$, $\kappa = 1.440.10^{-4}$, $Fr = 0.8476$,$\theta = 6.4°$

An important feature of this experiment is that, for different imposed frequencies, the generated wave displays significantly different features (presented in figure 4). For higher frequencies, the front and tail of the waves become closer which hinders the development of the wave precursors and may lead to strong interaction between the successive pulses. In order to simulate the experiments of Liu & Gollub, we consider the following initial condition

$$h(\tilde{x},0) = \eta(\tilde{x},0) = U(\tilde{x},0) = 1, \quad w(\tilde{x},0) = p(\tilde{x},0) = 0 \tag{61}$$

which corresponds to the Nusselt flow solution. The total numerical domain expands from $\tilde{x}_L = 0$ to $\tilde{x}_R = 2m$, for which the boundary conditions are prescribed as follows

$$\begin{aligned}
&\text{At } x = 0: \quad h_0^n = \eta_0^n = 1 + 0.1\sin(2\pi f t^n), \quad u_0^n = 1, \quad w_0^n = 0.2\pi f\cos(2\pi f t^n), \quad p_0^n = (\eta_1^n - \eta_0^n)/\Delta x \\
&\text{At } x = L: \quad h_{N+1}^n = h_N^n \quad u_{N+1}^n = u_N^n, \quad \eta_{N+1}^n = \eta_N^n, \quad w_{N+1}^n = w_N^n, \quad p_{N+1}^n = p_N^n
\end{aligned}$$

The dimensionless frequency is given by $f = \tilde{f}L/\tilde{U}_N$, where $\tilde{f}$ is the imposed dimensioned frequency. In all the numerical tests presented hereafter for the Liu & Gollub's experiments, we take the following values of the model's parameters:

Physical constants	$g = 9.80\ m\ s^{-2}$	$\sigma = 0.067\ Kg\ s^{-2}$	$\nu = 6.28\times10^{-6}\ m^2\ s^{-1}$	$\rho = 1080\ Kg\ m^{-3}$	$\theta = 6.4°$	
Dimensionless Numbers	$Re = 19.33$	$F = 0.8476$	$We = 0.1858$	$\varepsilon = 6.07\times10^{-3}$	$\kappa = 3.866$	$\lambda = 3$
Reference quantities	$\tilde{h}_N = 1.279\ mm$	$\tilde{U}_N = 94.94\ mm\ s^{-1}$	$L = 210.5\ mm$			
Relaxation parameters	$\alpha = 6.07\times10^{-3}$	$\beta = 2.243\times10^{-7}$				

Table 1: Summary of the model parameters' values used in the Liu & Gollub's experiments. The relaxation parameters are taken equal to $\alpha = \varepsilon$ and $\beta = \varepsilon^3$.

The numerical results are given below for both proposed formulations.

4.2.1. Hyperbolic-parabolic model

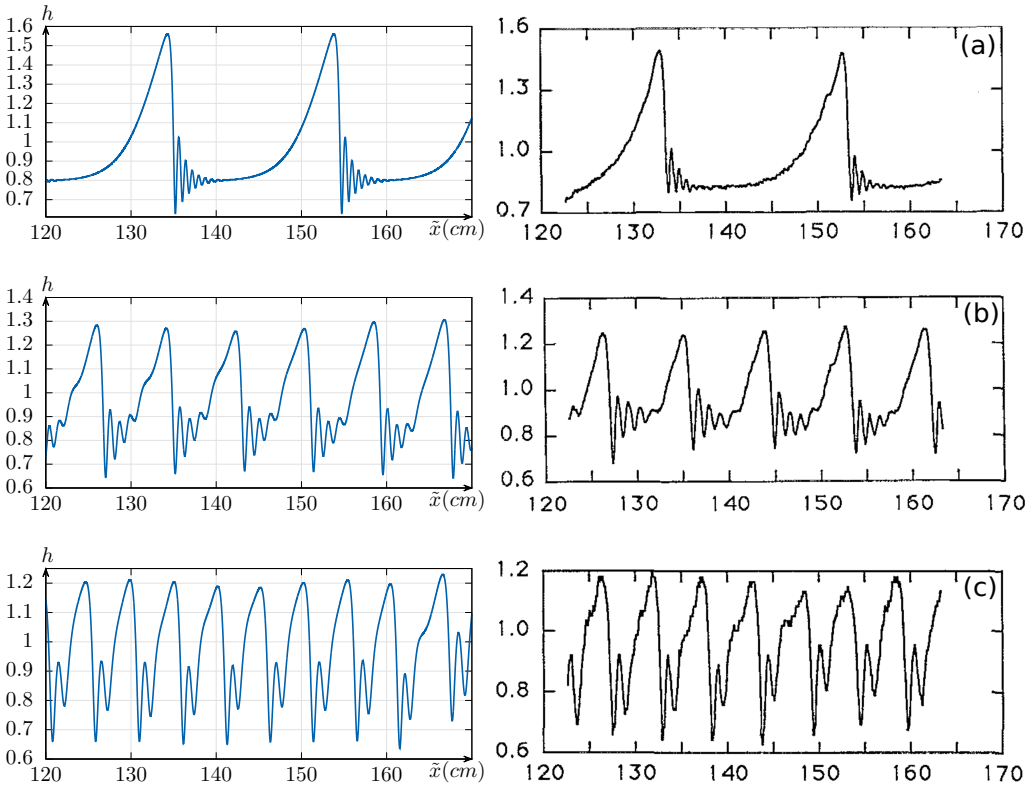

Figure 4: Experimental results of Liu & gollub [31] (right) along the obtained numerical results (left), for different forcing frequencies, respectively equal to $(a) : \tilde{f}_1 = 1.5Hz$, $(b) : \tilde{f}_2 = 3.0Hz$ and $(c) : \tilde{f} = 4.5Hz$. The number of mesh points is $n = 40000$. Experimental results figures are reprinted from Jun Liu and J. P. Gollub. Solitary wave dynamics of film flows. *Physics of Fluids*, 6(5):1702–1712, 1994., with the permission of AIP Publishing.

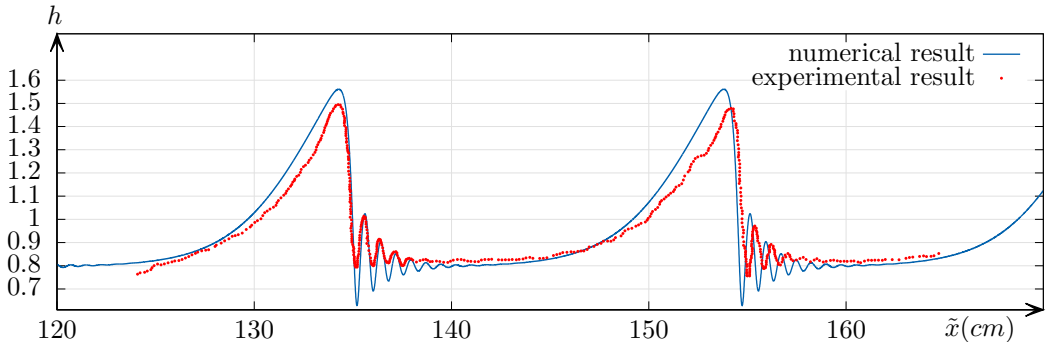

Figure 5: Superimposed numerical simulation with the experimental result for $\tilde{f} = 1.5Hz$.

Remark 4.1. *It may seem that the value* $Re = 19.33$ *used here is in discrepancy with the one used in [31] which is* $Re' = 29$. *The equality* $Re' = 3Re/2$ *is due to the fact that both Reynolds numbers are defined with different reference velocities. In fact, we consider here as reference velocity the averaged equilibrium*

velocity over the depth $\tilde{U}_N$, while the reference value used in [31] is the value of the velocity at the water surface $\tilde{u}_N(h_N) = 3\tilde{U}_N/2$. (See equations (33) and (32))

For the different forcing frequencies, the numerically simulated waves display similar features to the experimental measures for the chosen values of $\alpha = \varepsilon$ and $\beta = \varepsilon^3$. The agreement is qualitatively very good. One can see on figure 5 that the amplitude and the wavelength of both the wave peak and the capillary ripples, are approximately well recovered through the augmented model for the chosen values of α and β.

4.2.2. *Fully hyperbolic model*

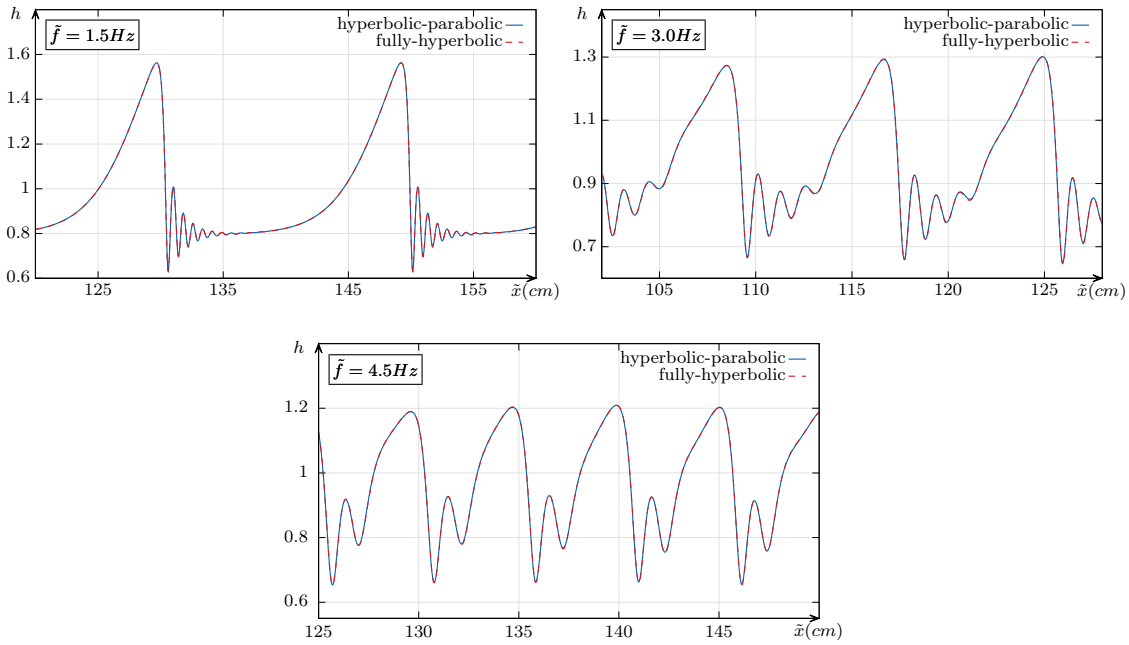

Figure 6: Comparison of the wave profiles for different frequencies. The blue continuous line stands for the hyperbolic-parabolic model. The red dashed line represents the fully hyperbolic formulation. Number of mesh points is $n = 10000$.

As displayed in figure 6, the results of both models are in agreement. Due to the additional stiff source term coming for the Rayleigh dissipation function, there is a phase error between both formulations. An approximate measurement of this shift error shows that it decreases with higher frequencies. Indeed, the values of the shift are given for the frequencies $\tilde{f}_1$, $\tilde{f}_2$ and $\tilde{f}_3$ respectively by $\Delta\tilde{x}_1 \simeq 22cm$, $\Delta\tilde{x}_2 \simeq 3.4cm$ and $\Delta\tilde{x}_3 \simeq 0$. Since, we are mainly concerned with the wave profiles, this phase error is suppressed in the previous comparison, by slightly shifting one of the numerical solutions. For reference, a comparison where the phase shift is the clearest to observe is given on figure (7)

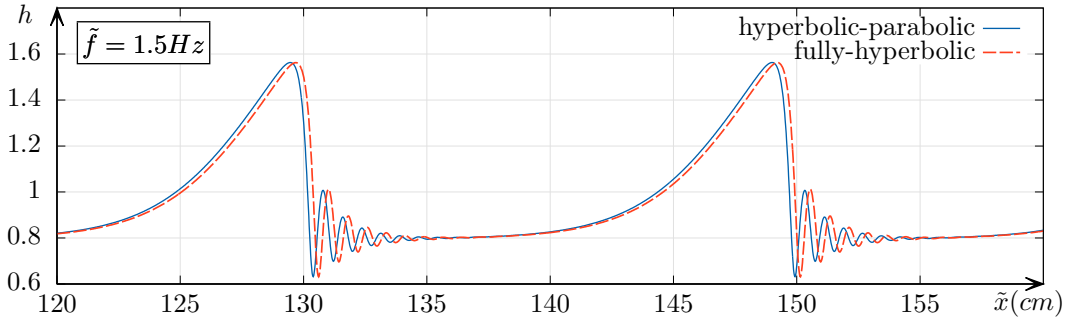

Figure 7: Comparison of both numerical solutions, including the phase shift for $\tilde{f} = 1.5Hz$. Number of mesh points is $n = 10000$.

4.3. Nonlinear surface tension model

We compare with the results obtained in [35] for a Gaussian initial data. It offers the advantage of being one of the few tests that was compared for both linear and nonlinear surface tensions in the non-stationary case. Thus, for the setting of this test, we consider the following Lagrangian, in dimensioned variables

$$\mathcal{L} = \int_{\Omega_t} \left(\frac{1}{2}\tilde{h}\tilde{U}^2 - \frac{1}{2}g\tilde{h}^2 - \frac{\sigma}{\rho}\left(\sqrt{1+\tilde{h}_{\tilde{x}}^2} - 1 \right) \right) d\Omega \tag{62}$$

to which corresponds, in augmented variables, the Lagrangian :

$$\mathcal{L} = \int_{\Omega_t} \left(\frac{1}{2}\tilde{h}\tilde{U}^2 + \frac{1}{2}\tilde{\beta}\tilde{h}\tilde{w}^2 - \frac{1}{2}g\tilde{h}^2 - \frac{\sigma}{\rho}\left(\sqrt{1+\tilde{p}^2} - 1 \right) + \frac{\tilde{h}}{2\tilde{\alpha}}\left(1 - \frac{\tilde{\eta}}{\tilde{h}} \right)^2 \right) d\Omega \tag{63}$$

We consider the initial data

$$\tilde{h}(\tilde{x},0) = \tilde{\eta}(\tilde{x},0) = h_0 + h_1 e^{-\frac{x^2}{2(b/b_0)^2}},\ \tilde{U}(\tilde{x},0) = 0,\ \tilde{p}(\tilde{x},0) = -\frac{h_1}{(b/b_0)^2}\tilde{x}e^{-\frac{x^2}{2(b/b_0)^2}},\ \tilde{w}(\tilde{x},0) = 0 \tag{64}$$

where h_0 is the water elevation at rest. b, b_0 and h_1 are parameters that define the shape of the Gaussian deformation as can be seen in figure 8.

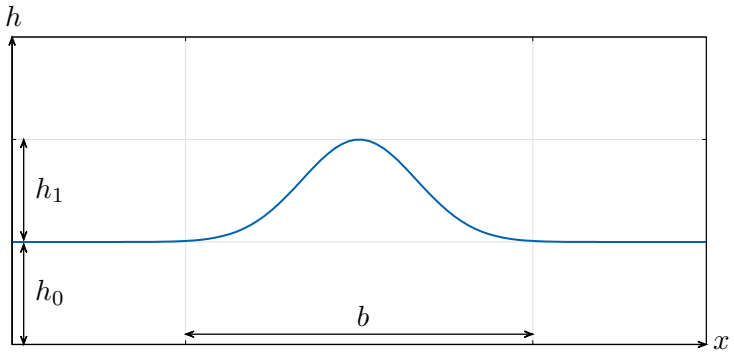

Figure 8: Shape of the Gaussian initial data.

Starting from the initial condition (64), we compute the time evolution of the deformation, which generates both gravity and capillary waves. For the simulation, we take a domain of $L = [-50mm, 50mm]$. The numerical results, at $t = 5ms$, is displayed in figure 9, with both linear and nonlinear capillarity terms :

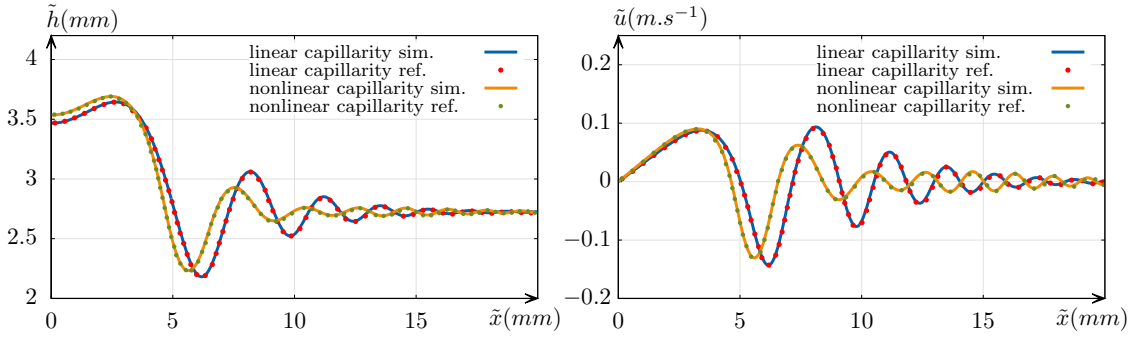

Figure 9: Comparison of the obtained numerical results (solid lines) with the converged numerical solutions proposed in [35] (dots), for the Gaussian initial data (64) at $t = 5ms$. Parameters used here are $g = 9.81m.s^{-2}$, $\sigma = 0.0728Kg.s^{-2}$, $\rho = 1000Kg.m^{-3}$, $h_0 = h_1 = 2.725\ mm$, $b = 1.5h_1$ and $b_0 = 4.29193$. $\tilde{\alpha} = 10^{-3}m^{-2}s^2$ and $\tilde{\beta} = 10^{-5}$. Results are shown with a mesh resolution of $n = 5000$ for the whole domain.

The shown results are obtained by using the same ARS(2,2,2) scheme. The cfl is set to 0.8. Unlike what was used in [35], there is no need to adjust the cfl to be able to capture the capillary waves, as the characteristic velocities of the model, naturally include the fast oscillations scale. The comparison shows a perfect agreement, in terms of wave amplitude, wave frequency and wave speed. The comparison of $\tilde{p}$ with $\tilde{h}_{\tilde{x}}$, computed through centered finite differences is given in the next figure for both capillarity forms:

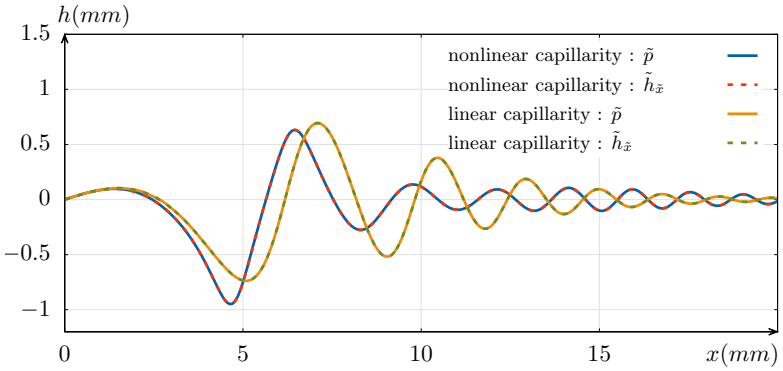

Figure 10: Comparison of $\tilde{h}_{\tilde{x}}$ (dashed lines) and $\tilde{p}$ (continuous lines) for the same values as above for both linear and nonlinear surface tension models. The curves coincide perfectly.

This test shows that the numerical results obtained for both linear and nonlinear surface tension models match perfectly with the converged numerical solutions of [35].This test shows that the augmented model in this setting, approximates the original model with excellent accuracy.

4.4. Mesh and relaxation convergence study

In order to demonstrate the convergence order of the used numerical method, we provide a convergence table (table 2) for the previous test with linearized surface tension. The reference solution in this case is a numerical solution obtained on a very fine mesh $n = 2^{16}$. The table shows that the convergence rate is indeed of second order. Figure 11 further illustrates the convergence of the solution .

N_x	$\epsilon_{L_2}(\rho)$	$\epsilon_{L_2}(u)$	$\epsilon_{L_2}(\eta)$	$\epsilon_{L_2}(p)$	$O_{L_2}(\rho)$	$O_{L_2}(u)$	$O_{L_2}(\eta)$	$O_{L_2}(p)$
2^9	1.11×10^{-2}	3.92×10^{-1}	1.10×10^{-2}	4.27×10^{-1}	–	–	–	–
2^{10}	2.69×10^{-3}	9.17×10^{-2}	2.71×10^{-3}	1.01×10^{-1}	2.04	2.09	2.02	2.07
2^{11}	5.42×10^{-4}	2.26×10^{-2}	5.38×10^{-4}	2.12×10^{-2}	2.31	2.01	2.33	2.25
2^{12}	1.18×10^{-4}	5.04×10^{-3}	1.32×10^{-4}	4.96×10^{-3}	2.19	2.16	2.02	2.09
2^{13}	2.84×10^{-5}	1.31×10^{-3}	3.38×10^{-5}	1.26×10^{-3}	2.06	1.94	1.97	1.96

Table 2: Convergence table for a Gaussian droplet breakup numerical solution, obtained by the second-order ARS (2,2,2) scheme. The ϵ_{L_2} denote the L_2 relative error and O_{L_2} represent the corresponding convergence order.

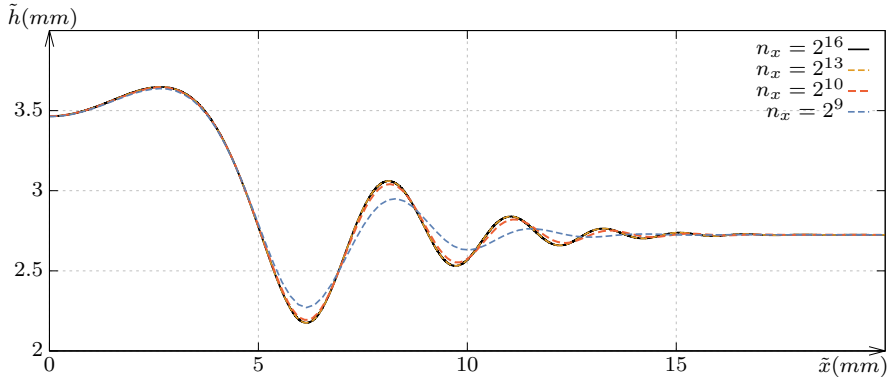

Figure 11: Mesh convergence test for the breakup of a gaussian droplet with linearized surface tension. Other parameters used here are the same as in figure 9

Convergence in the relaxation parameters requires a sufficiently refined mesh, since the scheme is not asymptotic preserving. In fact the fluxes contain stiff terms due to the relaxation and which are resolved explicitly in time. In figure 12, we show the same numerical solution for the gaussian droplet breakup, for several values of the relaxation parameters $\tilde{\alpha}$ and $\tilde{\beta}$ on two different meshes with resolutions $n = 2500$ and $n = 5000$. While, on the latter, one can observe a convergence trend in the sense that the numerical solution becomes independent on the choice of the penalty parameters for sufficiently stiff values, the former shows that insufficiently resolved meshes with stiff penalty parameters might result in dispersive numerical artifacts that pollute the numerical solution.

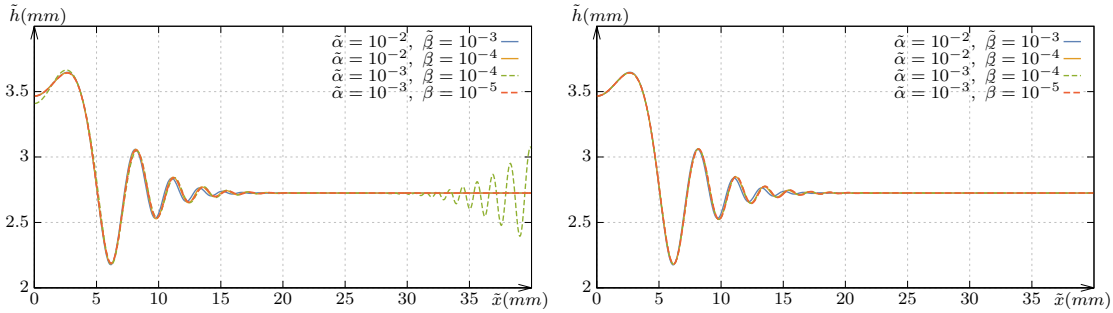

Figure 12: Numerical solution at $t = 5ms$ for the breakup of a Gaussian droplet on two different mesh resolutions of $n = 2500$ (left) and $n = 5000$ (right). The total computational domain is $[-50mm, 50mm]$ and other parameters used here are $g = 9.81m.s^{-2}$, $\sigma = 0.0728Kg.s^{-2}$, $\rho = 1000Kg.m^{-3}$, $h_0 = h_1 = 2.725\ mm$, $b = 1.5h_1$ and $b_0 = 4.29193$

Conclusion

We presented in this paper a common framework for thin films flows with capillarity and viscosity, allowing to obtain accurately approximate models with a convenient mathematical structure. The numerical results obtained by numerically solving the proposed systems of equations, has shown good agreement with both experimental results as well as reference numerical solutions, for both proposed formulations of viscosity. Besides, the method was also shown to be easily applicable to other formulations of surface tension terms that are more relevant when considered applications involve large gradients of fluid height. However, one of the disadvantages of this approach lies in the fact that it is unable to deal with flows involving dry or nearly dry regions. This is due to the fact that the maximum characteristic velocity tends to infinity when the fluid depth h goes to 0. The treatment of such cases will be left to future endeavors.

Acknowledgments

F.D. was funded by a *UniTN starting grant* of the University of Trento and funded by INdAM via a GNCS Grant for young researchers.

Appendix A. α and β scaling

In this part we show that the augmented model is asymptotically equivalent to the original equations, with a suitable choice of the relaxation parameters α and β. The starting point in this analysis is the Euler-Lagrange equation (43d). We multiply it by $\beta\eta$ in order to obtain

$$\frac{\eta}{\alpha}\left(1-\frac{\eta}{h}\right) = \beta\eta h\dot{w} - \eta\partial_x\left(\frac{\varepsilon^2\kappa}{F^2}p\right)$$

This implies

$$\eta = h + \frac{\kappa}{F^2}\varepsilon^2\alpha h\partial_x p - \alpha\beta h^2\dot{w}. \tag{A.1}$$

At this point, we assume that α and β are given in power laws of ε such that $\alpha = \varepsilon^{n_1}$ and $\beta = \varepsilon^{n_2}$ where the exponents $n_1, n_2 \geq 0$. Under this scaling, the latter equation writes

$$\eta = h + \frac{\kappa}{F^2}\varepsilon^{2+n_1} h\partial_x p - \varepsilon^{n_1+n_2} h^2\dot{w}. \tag{A.2}$$

Substituting (A.2) in the momentum equation (43b) allows us to write

$$\begin{aligned}\partial_t(hU) + \partial_x\left(hU^2 + \frac{2\lambda^2 h^5}{225} + \frac{h^2\cos\theta}{2F^2}\right) =& \frac{1}{\varepsilon Re}\left(\lambda h - \frac{3U}{h}\right) + \frac{9\varepsilon}{2Re}\partial_x(h\partial_x U) + \frac{\varepsilon^2\kappa}{F^2}hh_{xxx} \\ &- \varepsilon^{n_2}\left(h^2\dot{h}\right)_x + \varepsilon^{n_1+4}\frac{\kappa}{F^4}h\left(h_x h_{xxx} + (h_x h)_{xxx}\right) + o\left(\varepsilon^{n_2}\right) + o\left(\varepsilon^{4+n_1}\right)\end{aligned} \tag{A.3}$$

Equation (A.3) is asymptotically equivalent to (43b) if the leading order error terms in ε are of order larger than 2 *i.e.* n_2 is larger than 2. The most straightforward choice corresponds to $n_2 = 3$, meaning $\beta = O(\epsilon^3)$.

Appendix B. The Rayleigh dissipation function

Given a generic Lagrangian

$$\mathcal{L} = \int_{\Omega_t} L(q_1, \dot{q}_1, q_2, \dot{q}_2, ...)\, d\Omega \tag{B.1}$$

one can include the effects of friction forces directly to the Euler Lagrange equations by writing

$$\frac{d}{dt}\left(\frac{\partial L}{\partial \dot{q}_j}\right) - \frac{\partial L}{\partial q_j} = Q_j \tag{B.2}$$

where Q_j represents the non-conservative forces. In this context, it is convenient to define a scalar dissipation function $\mathcal{R}$ from which friction forces can be derived, similarly to how conservative forces are derived from a potential [30]. Such a function is often taken as a quadratic function in $\dot{q}$. One can then substitute Q_j in the previous equation so that it becomes

$$\frac{d}{dt}\left(\frac{\partial L}{\partial \dot{q}_j}\right) - \frac{\partial L}{\partial q_j} + \frac{\partial \mathcal{R}}{\partial \dot{q}_j} = 0. \tag{B.3}$$

In the context of our study, we choose the Rayleigh function as

$$\mathcal{R} = \frac{3U^2}{2h\varepsilon Re} + \frac{9\varepsilon w^2}{4\eta Re} \tag{B.4}$$

This only induces changes to the Euler-Lagrange equations

$$\partial_t(hU) + \partial_x\left(hU^2 + \frac{2\lambda^2}{225}h^5 + \frac{\cos\theta}{2F^2}h^2 + \frac{\eta}{\alpha}\left(1-\frac{\eta}{h}\right) + \frac{\varepsilon^2\kappa}{2F^2}p^2\right) = \frac{\lambda h}{\varepsilon Re} \underbrace{-\frac{3U}{h\varepsilon Re}}_{-\mathcal{R}_U} \tag{B.5a}$$

$$\partial_t(hw) + \partial_x\left(hwU - \frac{\varepsilon^2\kappa}{\beta F^2}p\right) = \frac{1}{\alpha\beta}\left(1-\frac{\eta}{h}\right) \underbrace{-\frac{9\varepsilon w}{2\beta\eta Re}}_{-\partial_w\mathcal{R}} \tag{B.5b}$$

The choice of the dissipation function is not arbitrary, as it is taken to preserve the asymptotic equivalence of our system with the PDE (37) given in section 3.1. This can be proven as follows. First we rewrite the term $\frac{\eta}{\alpha}\left(1-\frac{\eta}{h}\right)$

$$\frac{\eta}{\alpha}\left(1-\frac{\eta}{h}\right) = -\eta\partial_x\left(\frac{\varepsilon^2\kappa}{F^2}p\right) + \frac{9\varepsilon w}{2Re} + \beta\eta h\dot{w}. \tag{B.6}$$

Under the same notation of the previous appendix, replacing the latter expression into the momentum equation (B.5a) allows us to write

$$\begin{aligned}\partial_t(hU) + \partial_x\left(hU^2 + \frac{2\lambda^2h^5}{225} + \frac{h^2\cos\theta}{2F^2}\right) =& \frac{1}{\varepsilon Re}\left(\lambda h - \frac{3U}{h}\right) - \partial_x\left(\frac{9\varepsilon w}{2Re}\right) + \frac{\varepsilon^2\kappa}{F^2}hh_{xxx} \\ &- \varepsilon^{n_2}\left(h^2\dot{h}\right)_x + \varepsilon^{n_1+4}\frac{\kappa}{F^4}h\left(h_xh_{xxx} + (h_xh)_{xxx}\right) + o\left(\varepsilon^{n_2}\right) + o\left(\varepsilon^{4+n_1}\right)\end{aligned}$$

Thus, by virtue of the previous analysis, this formulation is compatible with the PDE (37) as long as the term $\frac{9\varepsilon w}{2Re}$ is asymptotically consistent with $-\frac{9\varepsilon}{2Re}h\partial_xU$. This can be shown as follows. First, by using equation (B.6) we can express η as a function of h then apply a material derivative to obtain

$$w = \dot{h} + \frac{9\varepsilon^{1+n_1}}{2Re}\left(\partial_t\left(wh/\eta\right) + u\partial_x\left(wh/\eta\right)\right) - \varepsilon^{n_1+n_2}(\partial_t(h^2\dot{w}) + u\partial_x(h^2\dot{w})) + o(\varepsilon^{1+n_1}). \tag{B.7}$$

Plugging this expression into the previous expansion of the momentum of equation and recalling that $\dot{h} = -h\partial_xU$ by virtue of the mass conservation equation, we can finally write

$$\begin{aligned}\partial_t(hU) + \partial_x\left(hU^2 + \frac{2\lambda^2h^5}{225} + \frac{h^2\cos\theta}{2F^2}\right) =& \frac{1}{\varepsilon Re}\left(\lambda h - \frac{3U}{h}\right) + \frac{9\varepsilon}{2Re}\partial_x(h\partial_xU) + \frac{\varepsilon^2\kappa}{F^2}hh_{xxx} - \varepsilon^{n_2}\left(h^2\dot{h}\right)_x \\ &- \frac{81}{4Re^2}\varepsilon^{2+n_1}\left(\partial_t\left(wh/\eta\right) + u\partial_x\left(wh/\eta\right)\right) + o\left(\varepsilon^{n_2}\right) + o\left(\varepsilon^{2+n_1}\right)\end{aligned}$$

Thus, the asymptotic structure of the model (37) is conserved if and only if $n_2 > 2$ and $n_1 > 0$. We can take for example in this case $n_1 = 1$ and $n_2 = 3$.

Appendix C. Critical stability curve

We write the characteristic polynomial of the matrix $\mathbf{M}$ defined in equation (49), in terms of the variable $X = u_0 - c_p$

$$\frac{1}{\alpha\beta\varepsilon k^3} X\left(A_0 + A_1 X + A_2 X^2 + A_3 X^3 + A_4 X^4\right) = 0 \tag{C.1}$$

where the coefficients are given by

$$A_0 = \frac{6i}{Re} + C\varepsilon k + \frac{6i\alpha}{ReWe}k^2\varepsilon^2 + \frac{1+\alpha C}{We}k^3\varepsilon^3, \quad A_1 = \frac{3i}{Re} + \frac{3i\alpha}{ReWe}k^2\varepsilon^2$$
$$A_2 = -\left(\frac{6i\alpha}{Re}\beta k^2 + \left(1 + \beta k^2 + \alpha C\beta k^2\right)k\varepsilon + \frac{\alpha}{We}k^3\varepsilon^3\right), \quad A_3 = -\frac{3i\alpha\beta k^2}{Re}, \quad A_4 = \alpha\beta\varepsilon k^3$$

and $C = \frac{\cos\theta}{F^2} + \frac{2\lambda^2}{45}$ is a constant introduced only to lighten the expressions. Since we are looking for the critical curve $\mathrm{Im}(X) = 0$, this suggests that we search for nontrivial real roots of the characteristic polynomial (C.1). Thus, we discard the root $X = 0$ and consider a nonzero root $X \in \mathbb{R}^*$. Equating the real and imaginary parts of the characteristic polynomial to zero respectively, yields the equations

$$X^4 - \left(\frac{1}{\alpha} + C + \frac{\kappa}{\beta F^2} + \frac{1}{\alpha\beta k^2}\right)X^2 + \frac{C}{\beta}\left(\frac{\kappa}{F^2} + \frac{1}{\alpha k^2}\right) + \frac{\kappa}{\alpha\beta F^2} = 0 \tag{C.2a}$$

$$(X+2)\left(X^2 - \left(\frac{\kappa}{\beta F^2} + \frac{1}{\alpha\beta k^2}\right)\right) = 0 \tag{C.2b}$$

where X must be a common root to the two polynomials. Equation (C.2b) admits three real roots

$$X_1 = -2 \quad ; \quad X_{2,3} = \pm\sqrt{\frac{\kappa}{\beta F^2} + \frac{1}{\alpha\beta k^2}} \tag{C.3}$$

Substituting $X_{2,3}$ in (C.2a) yields

$$-\frac{1}{\alpha^2\beta} = 0 \tag{C.4}$$

which is not possible in our case. This leaves X_1 as the unique possible common root. Indeed, plugging the latter into equation (C.2a) yields

$$\frac{1}{k^2}\left(\frac{\kappa k^2}{F^2} - 4 + C\right) + \alpha\left(4\beta - \frac{\kappa}{F^2}\right)(4 - C) - 4\beta = 0 \tag{C.5}$$

By using the fact that $\lambda = \frac{Re\sin\theta}{F^2} = 3$, the parameter C can be reshaped into

$$C = \frac{\cos\theta}{F^2} + \frac{6Re\sin\theta}{45F^2}. \tag{C.6}$$

Further development and simplifications lead to the equation of the critical stability curve

$$\frac{\kappa k^2}{\sin\theta} + \mathrm{cotg}\theta - \frac{6}{5}Re + \left(\alpha\left(4\beta - \frac{\kappa}{F^2}\right)\left(\frac{6}{5}Re - \mathrm{cotg}\theta\right) - 4\beta\frac{F^2}{\sin\theta}\right)k^2 = 0 \tag{C.7}$$

References

[1] D. J. Benney, Long Waves on Liquid Films, Journal of Mathematics and Physics 45 (1-4) (1966) 150–155.
[2] V. Y. Shkadov, Wave flow regimes of a thin layer of viscous fluid subject to gravity, Fluid Dynamics 2 (1) (1967) 29–34.
[3] P. L. Kapitza, Wave flow of thin layers of viscous liquid. Part I. Free flow, Zhurnal Eksperimentalnoi i Teoreticheskoi Fiziki 18 (1948) 3–18.
[4] P. L. Kapitza, S. P. Kapitza, Wave flow of thin layers of viscous liquids. Part III. Experimental research of a wave flow regime, Zhurnal Eksperimentalnoi i Teoreticheskoi Fiziki 19 (1949) 105–120.
[5] G. L. Richard, M. Gisclon, C. Ruyer-Quil, J.-P. Vila, Optimization of consistent two-equation models for thin film flows, European Journal of Mechanics, B/Fluids 76 (1967) (2019) 7–25, ISSN 09977546.
[6] G. L. Richard, C. Ruyer-Quil, J.-P. Vila, A three-equation model for thin films down an inclined plane, Journal of Fluid Mechanics 804 (2016) 162–200, ISSN 14697645.
[7] C. Cattaneo, J. de Fériet, A. des sciences (France), Sur une forme de l'équation de la chaleur éliminant le paradoxe d'une propagation instantanée, Comptes rendus hebdomadaires des séances de l'Académie des sciences, Gauthier-Villars, 1958.
[8] I. Peshkov, E. Romenski, A hyperbolic model for viscous Newtonian flows, Continuum Mechanics and Thermodynamics 28 (1-2) (2016) 85–104.
[9] I. Peshkov, M. Pavelka, E. Romenski, M. Grmela, Continuum mechanics and thermodynamics in the Hamilton and the Godunov-type formulations, Continuum Mechanics and Thermodynamics 30 (6) (2018) 1343–1378.
[10] I. Peshkov, E. Romenski, M. Dumbser, Continuum mechanics with torsion, Continuum Mechanics and Thermodynamics 31 (5) (2019) 1517–1541.
[11] M. Dumbser, I. Peshkov, E. Romenski, O. Zanotti, High order ADER schemes for a unified first order hyperbolic formulation of Newtonian continuum mechanics coupled with electro-dynamics, Journal of Computational Physics 348 (2017) 298–342.
[12] S. Gavrilyuk, K.-M. Shyue, Hyperbolic approximation of the BBM equation, Nonlinearity 35 (3) (2022) 1447.
[13] N. Favrie, S. Gavrilyuk, A rapid numerical method for solving Serre–Green–Naghdi equations describing long free surface gravity waves, Nonlinearity 30 (7) (2017) 2718.
[14] F. Dhaouadi, N. Favrie, S. Gavrilyuk, Extended Lagrangian approach for the defocusing nonlinear Schrödinger equation, Studies in Applied Mathematics 142 (3) (2019) 336–358, ISSN 14679590.
[15] E. Madelung, Quantentheorie in Hydrodynamischer Form, Zeitschrift für Physik 40 (3) (1927) 322–326.
[16] J. D. van der Waals, The thermodynamic theory of capillarity under the hypothesis of a continuous variation of density, Journal of Statistical Physics 20 (2) (1979) 200–244.
[17] L. Rayleigh, On the theory of surface forces.—II. Compressible fluids, The London, Edinburgh, and Dublin Philosophical Magazine and Journal of Science 33 (201) (1892) 209–220.
[18] D. M. Anderson, G. B. McFadden, A. A. Wheeler, Diffuse-interface methods in fluid mechanics, Annual review of fluid mechanics 30 (1) (1998) 139–165.
[19] D. Bresch, F. Couderc, P. Noble, J.-P. Vila, New extended formulations of euler-korteweg equations based on a generalization of the quantum bohm identity, arXiv preprint arXiv:1503.08678 .
[20] P. Casal, La capillarité interne, Cahier du groupe français de rhéologie, CNRS VI 3 (1961) 31–37.
[21] P. Casal, Capillarité interne en mécanique des millieux continus, Compt. Rend 256 (3).
[22] P. Casal, H. Gouin, A representation of liquid-vapor interfaces by using fluids of second grade, in: Annales de Physique, vol. 13, 3–12, 1988.
[23] S. Benzoni-Gavage, S. Descombes, D. Jamet, L. Mazet, Structure of Korteweg models and stability of diffuse interfaces, Interfaces and free boundaries 7 (4) (2005) 371–414.
[24] S. Benzoni-Gavage, Planar traveling waves in capillary fluids, Differential and Integral Equations 26 (3-4) (2013) 439–485.
[25] P. Noble, J.-P. Vila, Stability theory for difference approximations of some dispersive shallow water equations and application to thin film flows, arXiv preprint arXiv:1304.3805 .
[26] B. Haspot, Existence of strong solutions for nonisothermal Korteweg system, in: Annales Mathématiques Blaise Pascal, vol. 16, 431–481, 2009.
[27] D. Bresch, M. Gisclon, I. Lacroix-Violet, On Navier-Stokes-Korteweg and Euler-Korteweg Systems: Application to Quantum Fluids Models .
[28] S. Busto, M. Dumbser, C. Escalante, N. Favrie, S. Gavrilyuk, On high order ADER discontinuous Galerkin schemes for first order hyperbolic reformulations of nonlinear dispersive systems, Journal of Scientific Computing 87 (2) (2021) 1–47.
[29] G. Lavalle, Integral modeling of liquid films sheared by a gas flow, Ph.D. thesis, 2014.
[30] H. Goldstein, C. Poole, J. Safko, Classical Mechanics, Addison Wesley, ISBN 9780201657029, 2002.
[31] J. Liu, J. P. Gollub, Solitary wave dynamics of film flows, Physics of Fluids 6 (5) (1994) 1702–1712, ISSN 10706631.
[32] U. M. Ascher, S. J. Ruuth, R. J. Spiteri, Implicit-explicit Runge-Kutta methods for time-dependent partial differential equations, Applied Numerical Mathematics 25 (2-3) (1997) 151–167, ISSN 01689274.
[33] E. F. Toro, Riemann solvers and numerical methods for fluid dynamics: a practical introduction, Springer Science & Business Media, 2013.
[34] B. Van Leer, Towards the ultimate conservative difference scheme III. Upstream-centered finite-difference schemes for ideal compressible flow, Journal of Computational Physics 23 (3) (1977) 263–275, ISSN 0021-9991.
[35] D. Bresch, N. Cellier, F. Couderc, M. Gisclon, P. Noble, G.-L. Richard, C. Ruyer-Quil, J.-P. Vila, Augmented skew-symmetric system for shallow-water system with surface tension allowing large gradient of density, Journal of Computational Physics 419 (2020) 109670.